Cyclotron-resonance measurements on p-type strained layer $Si_{1-x}Ge_x/Si$ heterostructures

S.L. Wong, D. Kinder, and R.J. Nicholas
Physics Department, Oxford University, Clarendon Laboratory, Parks Road, Oxford OX1 3PU, United Kingdom

T.E. Whall and R. Kubiak
Physics Department, University of Warwick, Conventry CV4 7AL, United Kingdom
(Received 30 January 1995)

Cyclotron resonance (CR) has been used to measure the effective mass of holes in a series of p-type modulation doped $Si_{1-x}Ge_x/Si$ heterostructures, in which x varies from 0.05 to 0.29, and the two-dimensional carrier density $p_s = (0.95 - 5.8) \times 10^{11}$ cm^{-2}. The measured masses for these samples are, to the best of our knowledge, the lowest yet reported, with a mass as low as $0.21m_0$ observed in a sample with $x = 0.05$ and $p_s = 0.95 \times 10^{11}$ cm^{-2}. The high quality of the samples (a 4 K hole mobility of up to 1.1×10^4 cm^2 V^{-1} s^{-1}) enables a clear resolution of two CR features corresponding to resonances from the lowest spin-split states, at the magnetic field where the filling factor changes from $1 < \nu < 2$ to the quantum limit ($\nu < 1$). Calculations of the Landau levels using a six-band $\mathbf{k}\cdot\mathbf{p}$ model give very good agreement with the experimental observations on the $x = 0.05$ sample, and provide a qualitative explanation of the change in mass with increasing Ge content.

Strained-layer systems not only provide a further degree of freedom in material combinations, but also give rise to novel reconstructions of the valence band, due to the lifting of the degeneracy of the light and heavy hole bands (LH and HH). This causes a significant reduction in the mass of the highest valence band,[1] leading to promising applications in high-mobility p-type transistors and low-threshold current quantum well lasers.[2] Recent rapid improvements in the quality of strained p-type $Si_{1-x}Ge_x/Si$ heterostructures[3–5] has given rise to much interest due to the possibility of integration with well-developed Si technology. Shubnikov–de Haas and cyclotron-resonance (CR) measurements[6–8] have been used to determine the hole effective mass (m^*_{hh}) in heavily doped $Si/Si_{1-x}Ge_x/Si$ quantum well structures, where values as low as 0.29 have been observed with a Ge content of $x = 0.37$. By contrast m^*_{hh} rose to 0.40, when a Ge content of $x = 0.13$ was used. In the present paper, we report cyclotron-resonance measurements on a series of p-type modulation doped $Si_{1-x}Ge_x/Si$ heterostructures, with x varying from $0.05 - 0.29$ and the two-dimensional carrier density, $p_s = (0.95-5.8)\times10^{11}$ cm^{-2}. We demonstrate that by the use of much lower doping levels very low m^*_{hh} can be observed, even for structures with a relatively small Ge content.

The series of $Si/Si_{1-x}Ge_x/Si$ single-side modulation doped quantum wells studied was grown by molecular beam epitaxy.[4] The structures were grown on Si substrates, with a 300-nm buffer layer, followed by a 300-Å strained $Si_{1-x}Ge_x$ quantum well layer (except for sample 39/42, which has a 220-Å-thick well), an undoped spacer layer, and finally a 500-Å boron-doped Si capping layer. The Ge content and electrical properties at 4 K (from magnetotransport measurements) are summarized in Table I. The chopped light source for far-infrared (FIR) transmission measurements was a CO_2-pumped molecular gas laser operating in the wavelength region of 47–1223 μm. Highly polished light pipes, reflecting

TABLE I. x and L_s are the Ge content in the alloy layer and the width of the spacer layer, respectively. The electrical properties are from magnetotransport measurements at 4 K. The next two columns give the average cyclotron masses of the lowest spin-split state and the field of the crossover of the CR feature. The final column contains the calculated field at which the quantum limit is reached.

Sample	x	L_s (Å)	Carrier density (10^{11} cm^{-2})	Mobility (cm^2 V^{-1} s^{-1})	m^*_{hh} (m_0)	$m^*_{hh,decoupled}$ (m_0)	B^{av}_{CR} (T)	B_{QL} (T)
32/12	0.05	200	0.95	9200	0.21, 0.25	0.204	5.1	3.9
32/9	0.08	200	1.6	8850	0.22, 0.27	0.198	6.5	6.6
31/11	0.11	200	1.8	10500	0.23, 0.28	0.193	7.9	7.4
30/39	0.12	200	2.1	8500	0.24, 0.30	0.191	8.5	8.7
32/13	0.12	200	2.5	9600	0.23, 0.29	0.191		10.3
30/47	0.13	100	4.0	7000	0.28, ~0.35	0.190	12	16.5
39/42	0.20	300	2.9	6100	0.22, 0.31	0.182	11.0	12.0
35/56	0.29	200	5.8	2200	~0.25	0.169		24.0

mirrors, and condensing cone optics were used to guide and focus the FIR onto the samples, which were placed inside an 18-T superconducting magnet and cooled to below 3 K. The magnetic field was along the sample growth direction. The percentage transmission of the FIR was monitored with a reference bolometer before the sample and a signal bolometer after it. Sample substrates were wedged to avoid interference effects.

Typical transmission spectra for the sample with $x = 0.05$ and the lowest carrier density are shown in the inset of Fig. 1. At a FIR wavelength of 699.4 μm, a clear, single CR feature is observed at 3.5 T. As the wavelength decreases to 458.5 μm, a double CR feature is seen at 4.6 T and 5.8 T, with the resonance at higher field gaining in strength as the wavelength decreases. Further decreasing the wavelength to 294.8 μm results in a complete transfer of strength to the higher resonance, and hence recovery of a single CR feature. The resonant excitation energy as a function of magnetic field is plotted in Fig. 1.

The points corresponding to the CR features can be fitted reasonably well by two straight lines passing through the origin. From the relation $E_{CR} = \hbar eB/m^*$ at CR, the fit gives effective masses of $0.21m_0$ and $0.25m_0$ for the lower- and higher-field features, respectively. Similar changing over of intensity from the lower to the higher CR feature is also seen in the other samples, except for sample 35/56 where only one broad feature is observed. The low mobility of sample 35/56 leads to relatively broad linewidths and hence suppresses the resolution of multiple transitions. The cyclotron masses found by similar linear fits for all the samples are summarized in Table I. The low-field, low mass values for these relatively lightly doped samples are in remarkably good agreement with the value of $m^*_{hh} = 0.23m_0$ for a sample with $x = 0.13$ and $p_s = 2.2 \times 10^{11}$ cm^{-2}, deduced from the temperature dependence of Shubnikov–de Haas oscillation amplitudes at lower magnetic fields ($\lesssim$3 T) by Whall *et al.*[5] The field at which the resonance changes from the lower- to higher-field feature, B^{av}_{CR}, is also given in Table I. These fields are approximately consistent with the field at which the filling factor $\nu = 1$.

The linear fit for the effective mass in the previous paragraph has taken a simplified view by describing the topmost valence band with a single average effective mass for each spin-split level, neglecting valence-band mixing. It is in fact well known that even in the presence of strain, the HH-LH mixing, though small near the zone center, becomes significant as the in-plane k vector or the number of filled Landau levels increases. Thus, the heavy hole effective mass is a function of both magnetic field and carrier density rather than being constant throughout.

k·p calculations of the valence-band Landau levels of the quantum well were performed with a six-band model, taking the HH, $(J, m_J) = (\frac{3}{2}, \pm\frac{3}{2})$, LH, $(J, m_J) = (\frac{3}{2}, \pm\frac{1}{2})$, and spin-orbit split-off, $(J, m_J) = (\frac{1}{2}, \pm\frac{1}{2})$ bands as the basis states. Unlike most III-V systems,[9] the spin-orbit split-off band cannot be neglected, due to the relatively small spin-orbit splitting ($\Delta = 44$ meV in Si).[10,11] The 6×6 Hamiltonian used was simplified from that in Ref. 12 by neglecting the inversion asymmetry-related terms. The boundary conditions adopted conserve the envelope function and envelope function current at the interfaces,[13] and the conventional assumption of Bloch function equality for well and barrier materials was used. The average valence-band offset and deformation potentials used to account for the strain effects were taken from Ref. 14. The Luttinger parameters of the alloy were evaluated from the band parameters A, B, and C calculated in Ref. 15. These parameters show significant bowing as a function of alloy composition. The axial approximation and an assumption that the well can be regarded as square were made in the calculation, the latter of which is only valid for structures with a very low carrier density. For higher carrier densities, the single-side doped structure will be more like a triangular well instead. As our

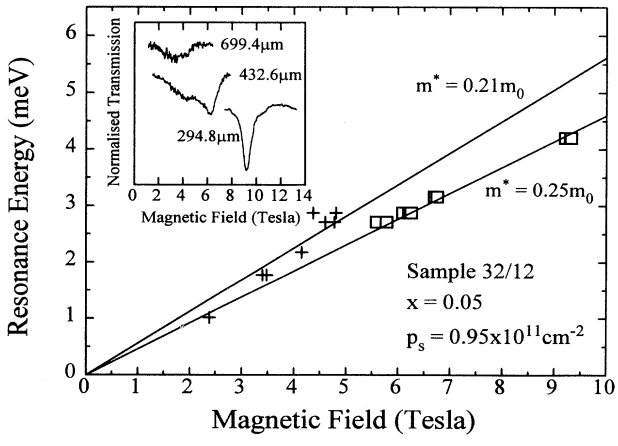

FIG. 1. Linear fits to the lower (crosses) and higher (squares) cyclotron resonances observed in sample 32/12. The fitted masses are indicated. The inset shows the transmission spectra at several FIR excitation wavelengths.

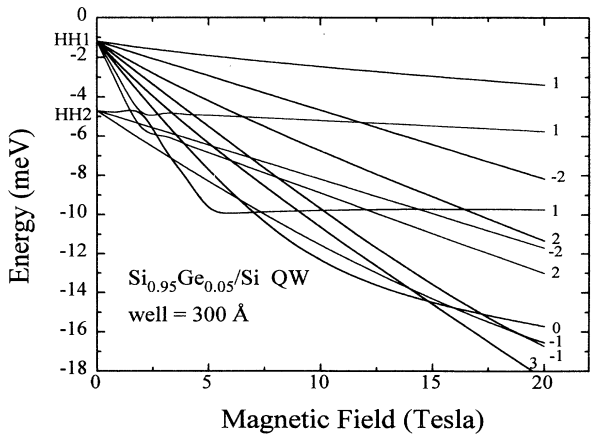

FIG. 2. The valence-band Landau levels for a 300-Å $Si_{0.95}Ge_{0.05}/Si$ quantum well. The zero of energy corresponds to the bottom of the heavy hole quantum well.

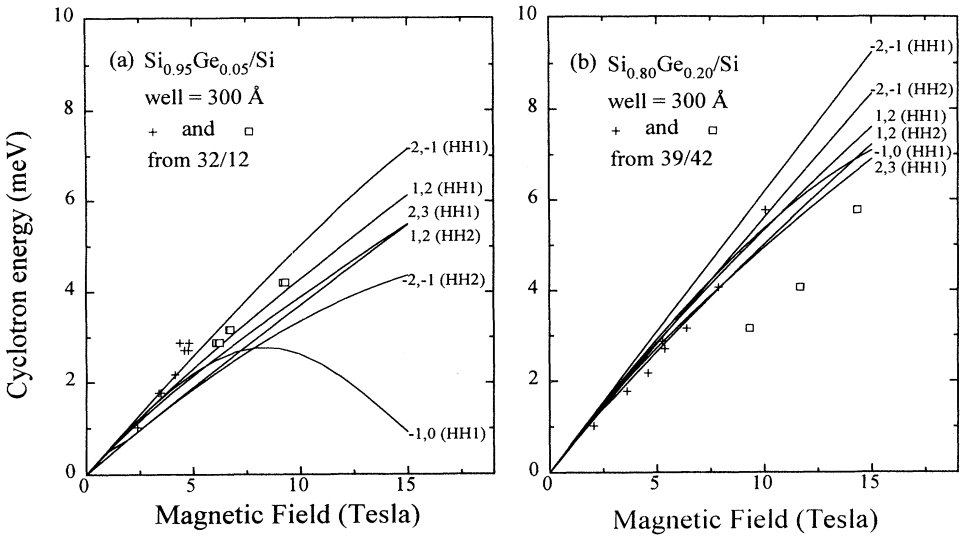

FIG. 3. Cyclotron energies for different transitions plotted against magnetic field, for (a) $x = 0.05$ and (b) $x = 0.20$. The crosses and squares are low- and high-field data points, respectively, from samples with the same Ge content as used in the calculation.

detailed discussion will be largely based on the $x = 0.05$ sample, which has a low carrier density, the above assumption is reasonable and the calculations for higher Ge contents will serve as a good qualitative comparison.

Figure 2 gives the calculated valence-band structure for a 300-Å $Si/Si_{0.95}Ge_{0.05}$ quantum well. The zero of energy corresponds to the bottom of the heavy hole well. The Landau levels are numbered as $n = -2, -1, 0, \ldots$, for the spin $m_J = -\frac{3}{2}$ and $n = 1, 2, 3, \ldots$, for the spin $m_J = +\frac{3}{2}$, in standard notation.[16] Due to the compressive strain in the well, the LH subbands are pushed higher up in the well with LH1 at -18.6 meV. Only the important levels (i.e., those at low energy) are shown, to avoid confusion. As seen clearly from the calculation, it is only within a small energy range close to the zone center (<5 meV) that the HH1 Landau levels can be described well by a constant effective mass. Beyond this, strong mixing with higher HH and LH subbands occurs.

To predict the CR energies, the statistics of the Landau levels must also be considered. The CR transitions satisfy the selection rule $\Delta n = \pm 1$. In the quantum limit $\nu < 1$ only $n = 1$ is populated. It should be noted that here $n = 1$ is the lowest HH1 Landau level (Fig. 2), unlike most other strained systems[9] where $n = -2$ is the lowest state. Thus, only the $1 \rightarrow 2$ transition is allowed, which does not have the lightest effective mass, in contrast to what is usually expected due to nonparabolicity. For $1 < \nu < 2$, holes also occupy the $n = -2$ level, and two transitions are possible: $1 \rightarrow 2$ and $-2 \rightarrow -1$, with relative intensities determined by the statistics and overlap integrals of the respective states. This is nicely demonstrated by our experimental observations, which show the effective mass falling once $n = -2$ is occupied. At higher ν, multiple transitions are always possible. Figure 3(a) plots the energies of the first few CR transitions. The $-2 \rightarrow -1$ transition has the larger slope and thus corresponds to the lighter mass. For the higher Landau level transitions, the slopes decrease with increasing Landau index and magnetic field. This partly explains why, in the samples studied previously,[6–8] much heavier masses were observed than those of the lightly doped samples studied here. The data for sample 32/12 with $x = 0.05$ is also plotted in Fig. 3(a), showing very good agreement with the calculations, particularly in the high-field limit when only the $1 \rightarrow 2$ transition is present.

We have also performed calculations on similar structures with higher Ge contents, which show a gradual decrease in the HH mass as the Ge content increases. This results from both the increasing HH-LH decoupling with increasing biaxial compression in the well and the in-

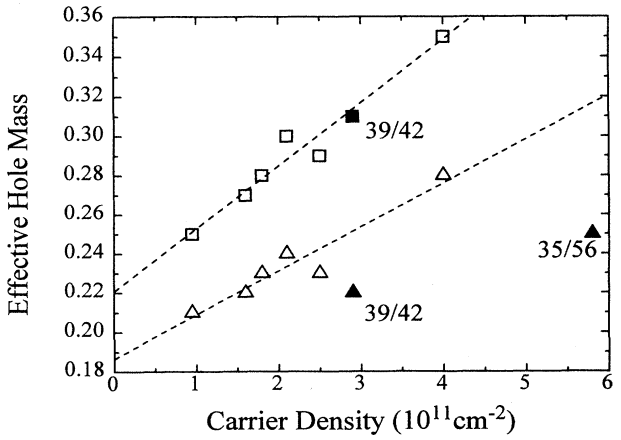

FIG. 4. Effective hole mass against carrier density for all samples. Triangles and squares represent the high- and low-field measurements, respectively, and the high Ge content samples are indicated by filled symbols. The data (excluding the high Ge content samples) has been linearly fitted, giving zero carrier density intercepts of $0.187m_0$ and $0.22m_0$.

crease in the Luttinger parameters with increasing Ge content. Comparison with the experimental data [Fig. 3(b)] shows that the calculated transition energies are increasingly too high as the Ge content increases. However, the experimental data is complicated by the fact that the increasing Ge content leads to a deepening of the well and a systematic increase in carrier density with Ge content. This causes an increasingly large deviation from the flat-band assumption and gives rise to stronger band bending effects, which our model has not taken into account. From Table I, it is clear that the measured mass of the samples with a low Ge content is actually less than that of those with a higher Ge content. This is due to the strong dependence of the effective mass on the carrier density, illustrated in Fig. 4, which plots the effective masses in both the high- and low-field limits. A clear trend can be seen, with both the high- and low-field masses increasing continuously. Using the group of samples with $x \lesssim 0.12$ extrapolation of the low field, low density limit suggests a band-edge mass of only $0.187m_0$. This value is in remarkably good agreement with the simple limit of a decoupled HH mass, given by $m^*_{\mathrm{hh,decoupled}} = (\gamma_1 + \gamma_2)^{-1} = 0.191$ for $x = 0.12$ as shown in Table I. It is also clear that the higher Ge content samples (39/42 and 35/56, with $x = 0.20$ and $x = 0.29$, respectively) have a significantly lower low-field mass from the $-2 \rightarrow -1$ transition than would be expected from the observed trend. This is, therefore, consistent with our calculations for the undoped (flat band) wells, which suggested a fall in effective mass with increasing Ge content.

In conclusion, we have observed a reduced in-plane hole effective mass in a series of strained $Si_{1-x}Ge_x/Si$ single-side doped quantum wells. A mass as low as $0.21m_0$ is observed in a sample with only 5% Ge and a relatively low doping level. Calculations of the CR transition energies which include HH-LH mixing show very good agreement with experiment for this sample. Higher Ge content samples have been measured and we have observed significantly lower masses than those reported for such systems. Calculations for higher Ge contents give a qualitative explanation for the observed behavior, but predict lower masses than those measured. This is believed to be due to the higher carrier densities in these samples. The calculations also indicate that masses significantly lower than 0.2 could be observed for high Ge content samples with a low carrier density.

[1] R.J. Warburton, G.M. Sundaram, R.J. Nicholas, S.K. Haywood, G.J. Rees, N.J. Mason, and P.J. Walker, Surf. Sci. **228**, 270 (1990).

[2] E.P. O'Reilly, Semicond. Sci. Technol. **4**, 121 (1989).

[3] R. People, J.C. Bean, D.V. Lang, A.M. Sergent, H.L. Störmer, K.W. Wecht, R.T. Lynch, and K. Baldwin, Appl. Phys. Lett. **45**, 1231 (1984).

[4] T.E. Whall, D.W. Smith, A.D. Plews, R.A. Kubiak, P.J. Phillips, and E.H.C. Parker, Semicond. Sci. Technol. **8**, 615 (1993).

[5] T.E. Whall, N.L. Mattey, A.D. Plews, P.J. Phillips, O.A. Mironov, R.J. Nicholas, and M.J. Kearney, Appl. Phys. Lett. **64**, 357 (1994).

[6] P.J. Wang, F.F. Fang, B.S. Meyerson, J. Norcera, and B. Parker, Appl. Phys. Lett. **54**, 2710 (1989).

[7] J.P. Cheng, V.P. Kesan, D.A. Grutzmacher, T.O. Sedgwick, and J.A. Ott, Appl. Phys. Lett. **62**, 1522 (1993).

[8] J.P. Cheng, V.P. Kesan, D.A. Grutzmacher, and T.O. Sedgwick, Appl. Phys. Lett. **64**, 1681 (1994).

[9] S.L. Wong, R.J. Warburton, R.J. Nicholas, N.J. Mason, and P.J. Walker, Phys. Rev. B **49**, 11 210 (1994).

[10] B. Gil, P. Lefebvre, P. Boring, K.J. Moore, G. Duggan, and K. Woodbridge, Phys. Rev. B **44**, 1942 (1991); B. Gil, L.K. Howard, D.J. Dunstan, P. Boring, and P. Lefebvre, *ibid.* **45**, 3906 (1992).

[11] C.Y-P. Chao and S.L. Chuang, Phys. Rev. B **46**, 4110 (1992).

[12] M.H. Weiler, in *Defects, (HgCd)Se, (HgCd)Te*, edited by R.K. Willardson and A.C. Beer, Semiconductors and Semimetals Vol. 16 (Academic, New York, 1981), p. 119.

[13] R. Eppenga, M.F.H. Schuurmans, and S. Colak, Phys. Rev. B **36**, 1554 (1987).

[14] C.G. Van de Walle, Phys. Rev. B **37**, 1871 (1987).

[15] K. Takeda, A. Taguchi, and M. Sakata, J. Phys. C **16**, 2237 (1983).

[16] A. Fasolino and M. Altarelli, in *Two Dimensional Systems: Heterostructures and Superlattices*, edited by G. Bauer, F. Kuchar, and H. Heinrich, Springer Series in Solid-State Physics Vol. 53 (Springer-Verlag, Berlin, 1984), p. 176.